

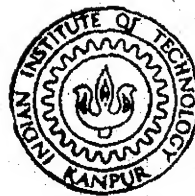
ROLLING AND RECRYSTALLIZATION BEHAVIOUR OF BORON DOPED Ni_3Al

By

RAGHUVIR PRASAD MATHUR

ME
MME
1991

M
MAT
ROL



DEPARTMENT OF METALLURGICAL ENGINEERING
INDIAN INSTITUTE OF TECHNOLOGY KANPUR
DECEMBER, 1991

ROLLING AND RECRYSTALLIZATION BEHAVIOUR OF BORON DOPED Ni_3Al

*A Thesis Submitted
In Partial Fulfilment of the Requirements
for the Degree of
MASTER OF TECHNOLOGY*

By
RAGHUVIR PRASAD MATHUR

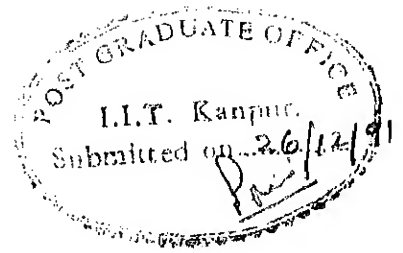
to the
DEPARTMENT OF METALLURGICAL ENGINEERING
INDIAN INSTITUTE OF TECHNOLOGY KANPUR
DECEMBER , 1991

4 FEB 1992


CENTRAL LIBRARY
U.S. AIR FORCE

Acc. No. A. 112807

CERTIFICATE



It is certified that the work contained in the thesis entitled '*Rolling and Recrystallization Behaviour of Boron Doped Ni₃Al*' by Mr. Raghuvir Prasad Mathur has been carried out under my supervision and that this has not been submitted elsewhere for the award of a degree.


(Dr. A.K. Jena)
Professor

Department of Metallurgical Engineering
Indian Institute of Technology
Kanpur

December 1991

ACKNOWLEDGEMENTS

I express my hearty gratitude to Professor A K Jena for his excellent guidance and constant advice throughout the course of this work. It was a great pleasure working under his guidance.

Thanks are due to The Director, DMRL, Hyderabad for his kind sponsoring of my M.Tech programme. It has been a good programme of study for which I am thankful to my teachers, Dr. G.S. Murthy, Dr. Jitendra Kumar, Dr. S.P. Gupta and Dr. Rajiv Shekhar.

I am thankful to Mr. K.P. Mukherjee, Mr. V. Kumar, Mr. M.N. Mungole and Mr. V.P. Gupta whose timely help at various stages of the work allowed me to complete the work as per time schedule. I owe my thanks to my friends Nagrajan, Satyam, Bhanu for help at various stage of work, as well as discussion on and off the subject.

My thanks are due to Shri Pant for typing this manuscript in an elegant form at a short notice.

Last, but not the least, I am sincerely indebted to my wife Mrs. Rajni Mathur for leaving the comfort of a settled life at Hyderabad for my M.Tech studies.

Raghuvir Prasad Mathur

CONTENTS

CERTIFICATE

ACKNOWLEDGEMENTS

LIST OF TABLES

LIST OF FIGURES

ABSTRACT

1. Introduction

2. Literature Review

2.1 Temperature and Compositional Stability

2.1.1 Binary Ni-Al System

2.1.2 Effect of ternary solutes on Ni_3Al

2.2 Structural aspects

2.2.1 Unit cell

2.2.2 Lattice parameter

2.2.3 Effect of processing

2.3 Diffusion

2.4 Transformation Kinetics

2.5 Mechanical Properties

2.5.1 Strength

2.5.2 Ductility

2.5.3 Creep

2.6 Scope of the present work

3. Experimental Procedure

3.1 Alloy preparation

3.1.1 Starting Materials

3.1.2 Melting

- 3.1.3 Homogenization
- 3.1.4 Annealing
- 3.2 Recrystallization
 - 3.2.1 Sample Preparation
 - 3.2.2 Rolling
 - 3.2.3 Recrystallization annealing
- 3.3 Optical Microscopy
- 3.4 Scanning Electron Microscopy
- 3.5 Thermal Analysis

4. Experimental Results

- 4.1 Homogenized Alloys
- 4.2 Rolling Behaviour
- 4.3 Recrystallization
 - 4.3.1 Alloy 'A' -15% deformation
 - 4.3.2 Alloy 'B' -20% deformation
 - 4.3.3 Alloy 'C' -30% deformation
- 4.4 DSC Measurements

5. Discussion

- 5.1 Rolling deformation behavior
- 5.2 Recrystallization behavior
- 5.3 Kinetics of recrystallization

6. Summary and Conclusions

REFERENCES

APPENDIX

LIST OF TABLES

- Table 1 Experimental data on the recrystallization kinetics and related values of intermetallic compounds and pure copper [32].
- Table 2 Composition and weight losses on melting in the alloy buttons melted for present study.
- Table 3 Rolling characteristics of boron doped Ni_3Al
- Table 4 Area fraction recrystallized at various recrystallization temperatures with time.

LIST OF FIGURES

- Fig.1. The binary Ni-Al phase diagram
- Fig.2(a) Electronic Chemical bonding natures and substitution behaviour of third element added to Ni_3Al
 (b) Solubility lobes for various ternary elements at 1273 K.
- Fig. 3 Auger spectra obtained from fractured surfaces of Ni_3Al specimen: (a) undoped Ni-24 at% Al (b) Ni-24 at% Al-0.5 wt% B. (c) same after 2 minutes of sputtering (d) Ni-25 at% Al-0.05 wt% B.
- Fig.4 Unit cell of ordered Ni_3Al (L1_2 structure)
- Fig.5 Temperature dependance of diffusivity of Ni in Ni_3Al in different works.
- Fig.6 Plots of room temperature tensile properties as a function of (a) boron concentration in Ni-24 at% Al (b) aluminium concentration in alloys doped with 0.05 wt% B.
- Fig.7 Scanning Electron Micrographs of structure of homogenized and annealed alloy 'C' at different magnification showing the single phase cast structure.
- Fig.8 Micrograph showing structure of homogenized and annealed alloy 'C' showing the directionality of grains [x50]
- Fig.9 Micrographs showing the structure of homogenised, annealed and 15% rolled alloy 'A' after a treatment at 1000°C for 1 hr (a) showing typical features of rolling (x70) (b) showing the deformation markings in the alloy [x350]
- Fig.10 Micrograph showing the structure of homogenised, annealed, 15% rolled and annealed alloy after 8% rolling showing intergranular crack [x 35].
- Fig.11 Micrograph showing the microstructure of homogenised and 30% rolled alloy 'C' showing the elongated grains [x 50]
- Fig.12 Micrograph showing the microstructure of 30% rolled and annealed ($850^\circ\text{C}/40$ min) alloy 'C' showing the grain separation. A few recrystallized grains are also seen [x 200].
- Fig.13 Micrographs showing the microstructure of 20% rolled alloy 'B' after a treatment at 1000°C for (a) 15 min. showing recrystallization at recrystallized grain boundary and grain edges (b) 135 min, showing almost complete recrystallization [x70]
- Fig.14 Micrographs showing the progress of recrystallization in 30% rolled alloy 'C' at 850°C (a) 20 min (b) 40 min (c) 60 min (d) 80 min (e) 100 min (f) 120 min [200x]

- Fig.15 Micrograph of the structure of 30% rolled alloy 'C' after recrystallization at 850°C for 120 min. The recrystallization is absent in one grain [$\times 50$]
- Fig.16 Micrographs showing the progress of recrystallization in 30% rolled alloy 'C' at 900°C for (a) 20 min (b) 40 min (c) 60 min [$\times 200$]
- Fig.17 Micrograph showing the progress of recrystallization in 30% rolled alloy 'C' at 925°C for (a) 20 min (b) 40 min (c) 60 min [$\times 200$]
- Fig.18 Plot showing the fraction recrystallized in 30% rolled alloy 'C' as function of time at various recrystallized temperatures.
- Fig.19 Differential scanning calorimetry plots for 20% rolled alloy 'B' at different heating rates.
- Fig.20 Plot of $-\ln[-\ln(1-X)]$ against $\ln t$ for calculation of Avrami exponent for recrystallization in 30% rolled Alloy 'C'
- Fig.21 Plots of $\ln t_x$ against $1/T$ for various fractions recrystallized for recrystallization in 30% rolled alloy 'C'.

ABSTRACT

Rolling of polycrystalline boron doped Ni_3Al was carried out on 2 mm thick slices. The rolling behaviour shows that intergrainular failure limits the ductility of these alloys. The ductility improved either with increased boron doping levels or by a slow cooling treatment which is supposed to cause segregation of boron at grain boundaries.

Annealing of cold rolled alloys in vacuum sealed ampoules caused recrystallization in samples rolled beyond 15% thickness reduction. Recrystallization in 30% deformation (thickness reduction) starts at high energy sites like grain boundaries, deformation bands etc. and can be described by Johnson-Mehl-Avrami (JMA) equation. The parameters of JMA equations suggests a 3-dimensional growth with reducing growth rates during recrystallization. The Avrami exponent is found to be 2.26 which compares well with the literature values. The activation energy is 118-146 KJ/mol in excellent agreement with the earlier reported values.

CHAPTER 1

INTRODUCTION

The high temperature structural materials commercially used today for aeroengine applications are mainly super alloys based on nickel, cobalt and iron. In the present world of improvement, the engine efficiency is of utmost importance. One of the ways to improve the engine efficiency is to raise the working temperature and as these alloys are being used closed to their melting points, it puts a severe limitation on further development with this class of material. Even though thermal barrier coatings and cooled structures are being tried, the key to the improvement lies in search for materials with better temperature capabilities. The ordered intermetallics are potential candidates in this regard as ordered structures tend to inhibit thermally activated processes. In addition, their lower densities reduce the weight of the structure and thus add further to the overall efficiency.

Amongst ordered intermetallics, nickel aluminide Ni_3Al has certain added advantages. It has a positive temperature coefficient for strength upto $600-700^\circ\text{C}$. It also possesses a homogeneity range in binary as well as ternary systems, giving flexibility for alloy design. Although its role in high temperature materials as precipitating phase γ' in Ni-base super alloys is well known, complete exploitation of its attractive properties in single phase material has not yet been possible. This is because of its extremely poor ductility and brittleness in polycrystalline forms. Recent knowledge that microalloying with boron can ductilise Ni_3Al has renewed interest in these alloys.

Thermal stability specially resistance to recrystallization gains importance not only from the processing point of view, but also during service. The combination of stress and temperature while in use may cause recrystallization. in a B-doped Ni_3Al has therefore been investigated and studies based on microscopic techniques as major tool are reported.

CHAPTER 2

LITERATURE REVIEW

2.1 Temperature and Compositional Stability

2.1.1 Binary Ni-Al system

The temperature and compositional stability in binary Ni-Al has been carried out using various techniques like X-ray analysis of slow cooled powders, thermal and micrographic analysis and magnetic measurements. Figure 1 shows the compiled Ni-Al phase diagram [1], based on these measurements. In the nickel-rich side, there has been slight disagreement regarding the phase boundaries, but the version given in Figure 1 is accepted as most proper [2]. The phase diagram reveals the presence of four intermetallic phases; orthorhombic Al_3Ni , hexagonal Ni_2Al_3 (formed peritectically on Al-rich side), bcc NiAl and fcc Ni_3Al . While Al_3Ni appears to be a line compound without a solubility range, others exist over composition ranges. Ni_3Al has a homogeneity range 23-27.5 at. % Al at 600°C , existing on both sides of stoichiometric composition. The homogeneity range, however reduces to about 3% at higher temperatures.

2.1.2 Effect of ternary solutes on Ni_3Al

As stated earlier, one of the advantage of Ni_3Al is its ability to form solid solutions with many elements. It forms substitutional solid solutions with elements having large atomic diameters, while smaller atoms like boron and carbon form interstitial solutions.

The properties of substitutional solutions depend greatly on what site the ternary additions substitutes.

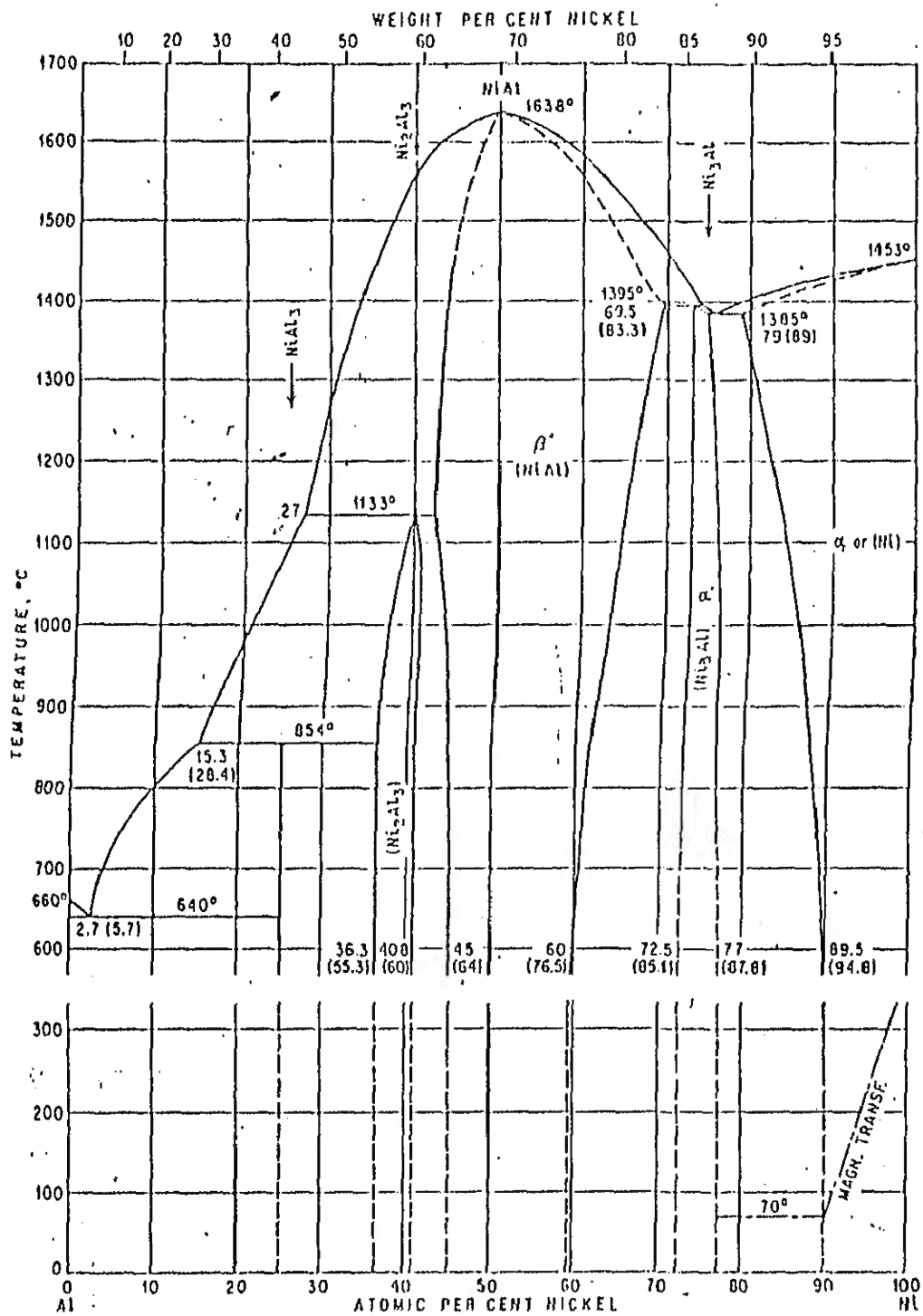


Fig.1. The binary Ni-Al phase diagram

Accordingly the substitutional solutes are classified in three broad categories [3].

- (i) Solutes replacing Ni-atoms (like Co, Cu, Pd, Pt and Sc)
: The solubility lobes of the ternary system shift from Ni side to ternary addition side.
- (ii) Solutes replacing Al atoms (like Si, Ti, Mn, V, Ge, Ga, Nb, Sb, Sn, Ta, Zn and Zr) : The direction of shift of solubility lobes is from Al side to ternary side.
- (iii) Solutes replacing both types of atoms (like Fe, Cr, Mo W and Hf) : The solubility lobes extend almost bisecting the quasi-binary section Ni_3Al , Ni_3X and $\text{Ni}_3\text{Al-X}_3\text{Al}$.

Solute like Fe, Hf, Cr etc. which lie mainly in 3rd group are commonly added to Ni_3Al for various improvements. Fe, for example, not only gives solid solution strengthening, but also reduces material cost and improves hot ductility and fabricability via formation of an ordered B2 phase [4]. The solubility limits of this group, however, shows a large variation in different studies. Solubility of Fe in Ni_3Al is reported to be as low as 4% [5] and more than 12% [6]. It is pointed out that Al/Ni ratio affects the solubility limits considerably [6]. Similar trends are seen for Hf having a solubility of about 8%, the curvature in solubility lobes, indicating the dependence of solubility on Al/Ni ratio [7].

Figure 2 presents the experimentally determined solubility lobes at 1273K [8], though phase diagrams based on thermodynamic calculations are also reported [9].

The principal interstitial solutes in Ni_3Al are boron and carbon. Boron has been studied in greater detail because of probable commercial applications. The room temperature solubility

(a)

Ni_3Al
(VIII)₃(III b.)

										III b	IV b	V b
III a	IV a	V a	VI a	VII a	VIII			I b	II b	Al	Si	
Sc	Ti	V	Cr	Mn	Fe	Co	Ni	Cu		Ga	Ge	
		Hf	Mo									Sb
		Ta	W									

Element substituting for Ni
 Element substituting for Al

(b)

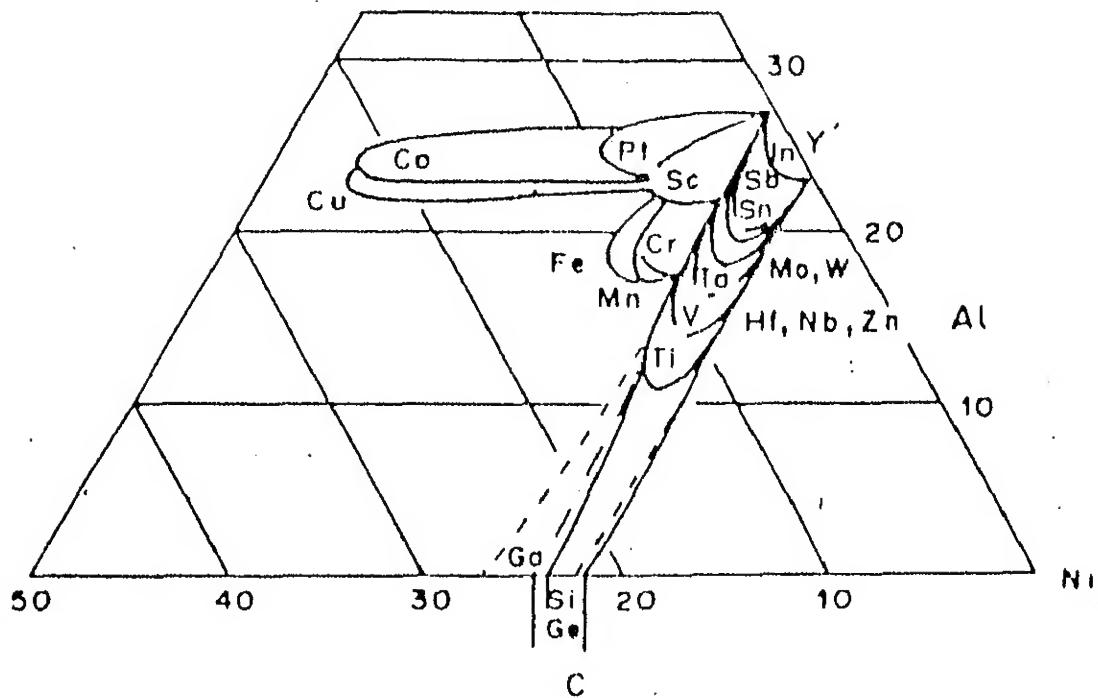


Fig.2(a) Electronic Chemical bonding natures and substitution behaviour of third element added to Ni_3Al
 (b) Solubility lobes for various ternary elements at 1273 K.

limit of boron in Ni_3Al is 0.3 ± 0.05 wt% [about 0.93 at%] beyond which boride of M_{23}B_6 type appears at 24% Al [10]. It increases to about 1.12% for stoichiometric composition [11]. The solubility limit can further be increased to 1.5% by rapid solidification techniques [12]. The actual distributions, however may be quite different from these average doping levels, because of the tendency of boron to segregate on grain boundaries. This has been confirmed indirectly by micro hardness measurements [13]. The Auger Electron Probe analysis of intergrainular area or fractured surfaces of undoped and B-doped Ni_3Al is shown in Figure 3 [10]. Based on the peak height ratio of boron to nickel it shows 10% boron levels in grain boundary region with average doping of 0.05% in Ni-24 Al alloys.

2.2 Structural Aspects

2.2.1 Unit Cell

The room temperature structure for Ni_3Al is an ordered cubic structure. It has Cu_3Au type structure (fcc based structure with structure beritch nomenclature L1_2). Figure 4 shows the schematic unit cell, nickel atoms occupy face centred positions and aluminum atom are at the cube corner. The stoichiometric composition is obviously 3:1 giving the formulae as Ni_3Al . The degree of ordering may differ from unity because the intermetallic exists over composition range on both sides of the stoichiometry.

Based on the lattice parameter and density variation with composition, Aoki and Izumi [14] has shown that in off-stoichiometric Ni-rich compositions, Ni-atoms occupy cube corner sites in addition to the face centred positions. Similarly Al-rich compositions have Al-atoms occupying a few face centred

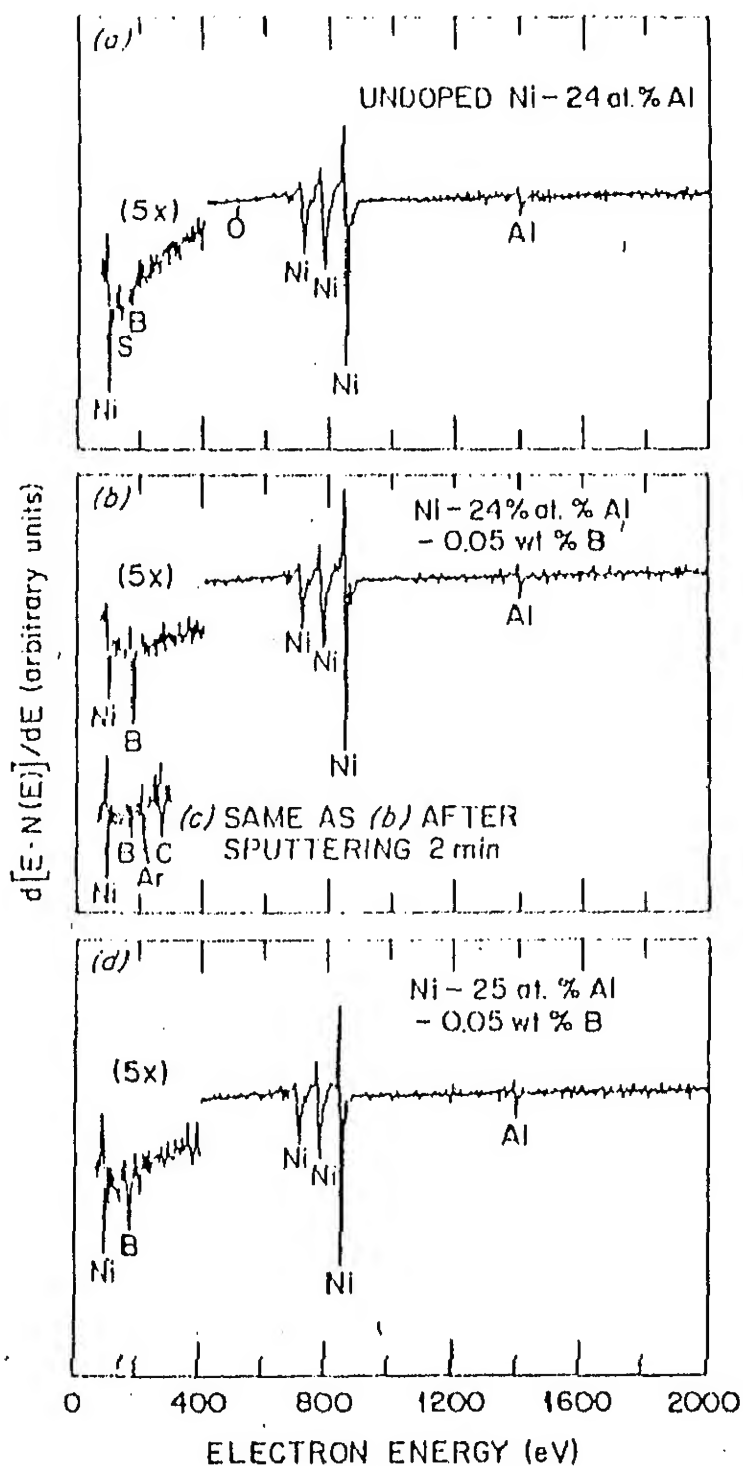


Fig. 3 Auger spectra obtained from fractured surfaces of Ni_3Al specimen: (a) undoped Ni-24 at% Al (b) Ni-24 at% Al-0.5 wt% B. (c) same after 2 minutes of sputtering (d) Ni-25 at% Al-0.05 wt% B.

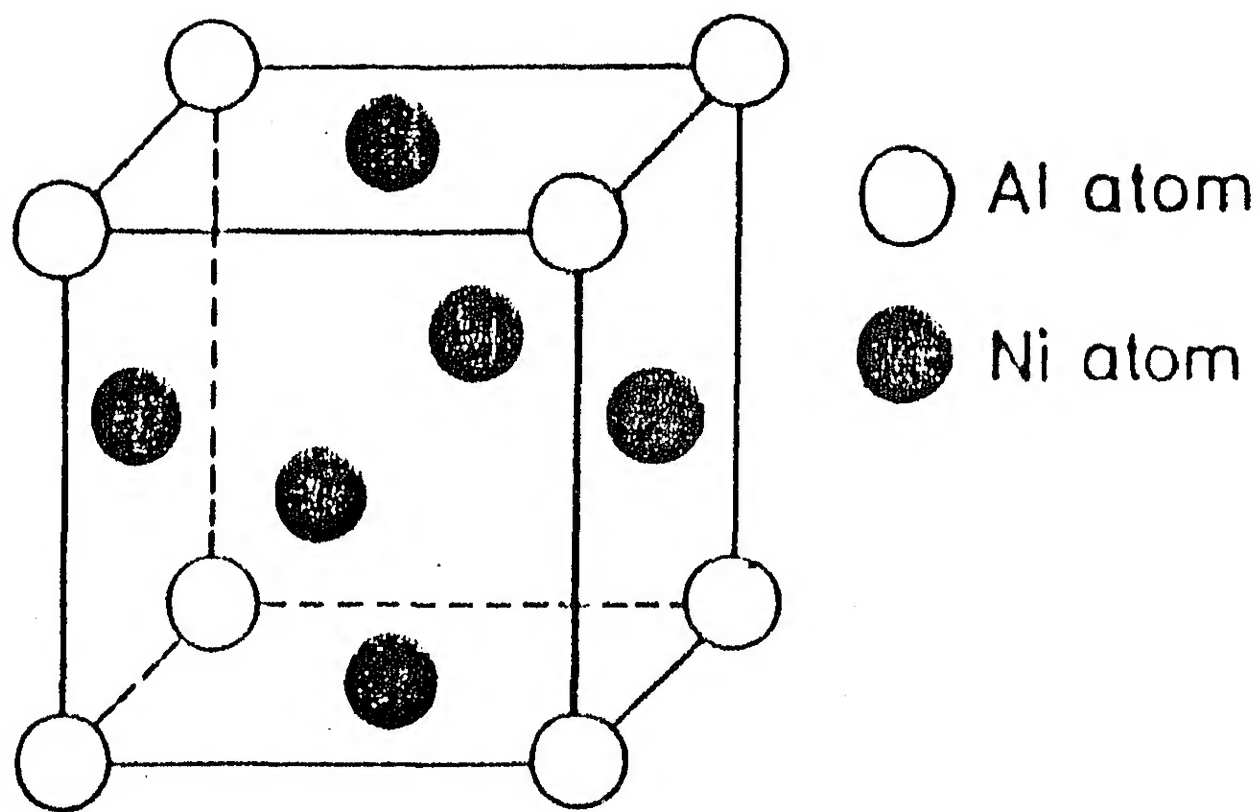


Fig.4 Unit cell of ordered Ni_3Al (L1_2 structure)

sites. Constitutional vacancies, however do not appear in all compositions.

Ni_3Al retains its ordered structure at elevated temperatures nearing melting points [14], changing to a disordered DO_{22} structure above critical temperatures.

2.2.2 Lattice Parameter

The earliest reported value of lattice parameter for Ni_3Al is $a = 3.589 \text{ \AA}$ for the stoichiometric composition [1]. The value reported for same composition by Guard and Westbrook [15] is 3.5700 \AA . Apparently the processing history affect the parameter. Cooling rates may also influence the parameter and hence it is difficult to compare the different studies [11]. The lattice parameter changes in binary Ni-Al has been studied by vapour deposition techniques [16]. The parameter varied linearly from 3.520 \AA for 0 Al to 3.560 \AA for 25% Al. Similar behaviour has been seen for bulk alloys [14].

Studies on B-doped Ni_3Al shows an increase in lattice parameter with increasing B under identical processing conditions. The value increased from 0.3552 nm for B-free alloys to 0.3560 nm for 0.5% B. Because of solutionising or redistribution of B, the lattice parameter varied for constant B level with heat treatments [17]. Rapidly solidified material also shows an increase in lattice parameter from 0.357 nm to 0.360 nm with boron variation from 0 to 6% [12]. The lattice parameter composition curve did not show any solubility limit though solubility limit was only 1.5% B. Addition of carbon also gives large changes in lattice parameter [12].

The lattice parameter variations of substitutional solutes from transition and B-sub group elements has also been studied [18].

2.2.3 Effect of Processing

Rapidly quenched Ni-22 Al revealed that fine anti phase domains outlined by disordered γ phase are surrounded by coarse domains. The trend is seen for B-free as well as B-doped alloys [19]. The behavior is attributed to micro segregation [20]. Coarse domains are associated with Al-rich interdendritic regions, where ordering temperatures are above solidus, whereas fine domain freeze from a disordered state directly. Rapid solidification in ternary alloys also gives ordered cells surrounded by disordered γ phase [21].

2.3. Diffusion

The diffusion of atoms in ordered intermetallics is comparatively difficult due to the constraints put up by ordering. This is the main source of the high temperature capabilities of these alloys. In Ni_3Al , diffusivity studies have been carried out both for B-free as well as B-doped alloys [22-24].

Early studies of Hancock [22] on undoped Ni_3Al show that while activation energy for diffusion of Ni in Ni_3Al does not change considerably with composition, preexponential factor is lower at stoichiometric composition. The atomic movement therefore appears to be nearest neighbour vacancy atom exchange. However the ratio of activation energy for migration E_m to the activation energy for diffusion ($E_m + E_f$) is more than 0.5 which suggests that like other ordered alloys diffusion is more

complicated than mere exchange of vacancies.

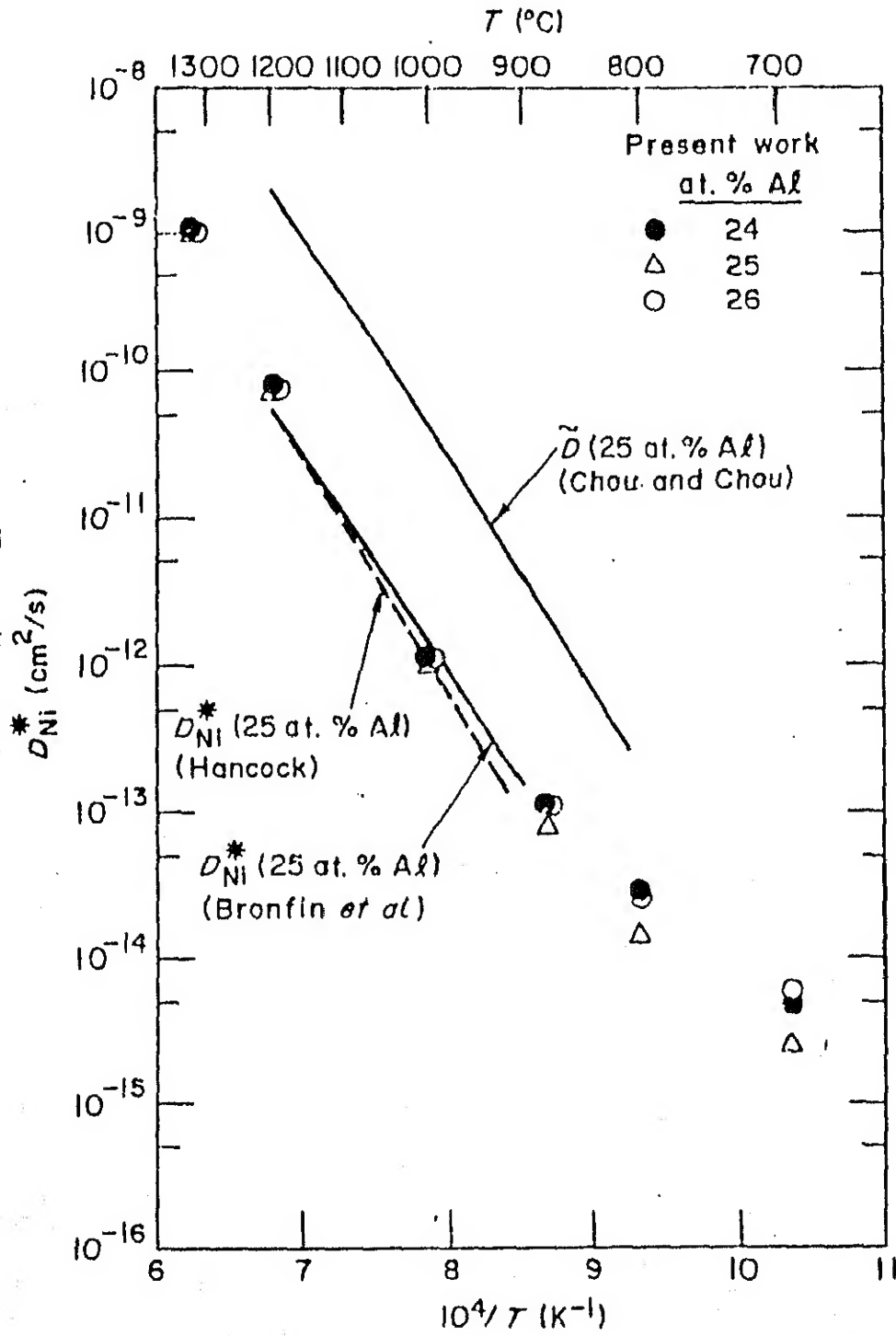
Tracer diffusion coefficient measurements shows that the diffusivity of Ni in Ni_3Al is independent of Al concentration at temperatures exceeding 1000°C . At lower temperatures, diffusion with lower activation energy is seen. This has been attributed to temperature independent vacancy concentration i.e. the constitutional vacancies. The Ni_3Al does not have constitutional vacancies on either side of the stoichiometry [14] and one possible reason of such vacancy concentration can be impurities like 3 wt ppm silicon in the sample [24]. Addition of boron increases the diffusivity of Ni. Nickel is known to co-segregate with B at grain boundaries [25] and hence increased diffusivity looks to be justified. Figure 5 shows the temperature dependance of diffusivity of Ni in Ni_3Al by various workers showing a good agreement at higher temperatures.

The diffusivity of Ni in Ni_3Al increases with addition of Co or Ge, though increase is less than that observed for D_{Ni}^* in pure Ni. This is attributed to different electronic configuration of Ni and Ni_3Al .

Grain boundary diffusivities measured using diffusion couple $\text{Ni}/\text{Ni}_3\text{Al} + \text{B}$, between temperature range $955\text{--}1124^\circ\text{C}$ [26] show that grain boundary diffusivities are 5-6 orders of magnitude higher than volume diffusivities. Activation energy, however, is higher for grain boundary diffusion.

2.4. Transformation Kinetics

The Kinetics for recovery recrystallization and grain growth have been studied for many Ll_2 compounds. The studies on



g.5 Temperature dependance of diffusivity of Ni in Ni_3Al indifferent works.

90% cold rolled Cu_3Au [27] revealed that rate of recrystallization above T_c is about 100 times higher than that below T_c . This suggests that recrystallization is inhibited by the ordered structure. The recrystallization texture formed below T_c is retained rolling texture while above T_c comprised of different texture component though recovery remained unaffected with the state of order, the activation energy being 51 kcal/mole both in ordered as well as disordered state. The activation energy for recrystallization was reported to be 27 kcal/mole for ordered state and 56 kcal/mole in disordered state, as compared to calculated activation energy for self diffusion as 46 kcal/mole.

Annealing behavior of Zr_3Al as well as binary Ni_3Al is well described by Avrami equations [30].

$$X_v = 1 - \exp(-bt^n).$$

Where X_v is the fraction recrystallized in time t , b and n are constants. Recrystallization in Zr_3Al for $X_v < 0.4$ shows the value of $n = 2$ with activation energy for 50% recrystallization as 2.2 eV [28]. For binary Ni_3Al with composition Ni-23.9 Al, exponent n was found to have a value between 1 and 2 without any definite linkage with temperature. The constant b , however showed a definite increase with temperature. The behaviour for n and b thus suggested unidirectional growth with either or both nucleation and growth rates increasing. Activation energy for a 50% recrystallization compared well with that of volume diffusion [29]. Such trends have been seen for B_2NiAl also [31].

B-doped Ni_3Al recrystallizes with a kinetics expressible by the Avrami equation. The Avrami exponent of the order of 2 compared well with binary Ni_3Al measurements, but the activation energy for recrystallization was quite lower 1.2 eV as compared with 3.4 eV in binary alloys [32]. Table 1 shows the compilation of available literature on these alloys [32].

Grain growth in pure Ni_3Al has been described by the power law relationship :-

$$\bar{d} = C t^n$$

Where \bar{d} is the average grain size after time t . C and n are empirical constants, depending upon the temperature. Constant 'C' includes a term for mobility of grains and hence increases with temperature. Exponent n , has a theoretical value of 0.5 in pure metals, however impediments in grain boundary migration reduced this value to practically used value of 0.33. The values for Zr_3Al [28] as well as Ni_3Al [29] were quite nearer to this value.

2.5 Mechanical Properties

Being a potential structural materials, Ni_3Al has been well characterized in terms of its mechanical properties. A larger interest however lies in its anomalous strength increase with temperature, improvement in ductility and creep properties essential for engine applications. These properties are reviewed here, other properties has been reviewed concisely by stoloff [4].

TABLE 1 Experimental data on the recrystallization kinetics and related values of intermetallic compounds and pure copper

Material	n	Q_R (eV)	Q_D (eV)	ΔH (J g ⁻¹)	Reference
Cu	1.1	1.1	2.0 ^a	1	18, 19
Ag	1.0	1.6	1.9 ^a	1.3	15, 19
Cu-2wt.%Au	—	—	—	0.6	15
Ag-0.2wt.%Al	—	—	—	0.6	15
Co ₃ Ti	0.6	1.8-2.5	—	—	12
Zr ₃ Al	2	2.2	—	—	11
NiAl	1-2	3.6	3.1 ^b	—	9
Ni ₃ Al [†]	1-2	3.4	3.2 ^c	—	10
B-doped Ni ₃ Al	2.2	1.2	—	3.2	Current work

n is the Avrami exponent. Q_R and Q_D are the respective activation energies for recrystallization and diffusion and ΔH is the stored energy of cold work.

^aSelf-diffusion [20].

^bNickel in a nickel compound [21].

^cNickel in a nickel compound [22].

2.5.1 Strength

Ni_3Al like many other Ll_2 compounds anomalous temperature coefficient for strength. Its flow stress increases with temperature to almost 3 fold the room temperature value at $600-700^\circ\text{C}$, beyond which a normal fall is seen. Both single crystals as well as polycrystalline forms shows such behavior. The flow stress increase is the result of thermally activated cross-slip of $[\bar{1} 01] \langle 111 \rangle$ screw dislocations to the (010) plane where they are sessile [33]. The barriers become irrelevant at higher temperatures due to massive cube slip on (010) plane and hence the fall of strength.

In addition to the strengthening due to long range ordering, Ni_3Al may be strengthened by normal techniques like grain boundary and solid solution strengthening.

Grain boundary strengthening in Ni_3Al can be expressed by Hall Petch type relationship

$$\sigma_y = \sigma_0 + k d^{-n}$$

The fitting of experimental data gives value of n to be 0.8 instead of Hall Petch exponent 0.5 [34]. Increased yield strength with finer grain size can be explained in terms of work hardening in Lüders Bands.

Solid solution strengthening for a large number of solutes has been studied [35]. Al and solutes substituting for Al gives an increase in strength while Ni and solutes substituting for Ni does not strengthen Ni_3Al , rather softening is seen in some cases. Elements which may go to either of Ni or Al sites have a larger range for strengthening. The potency for strengthening

with interstitial solutes like B or C is much higher than substitutional solutes [36].

2.5.2 Ductility

Ni_3Al shows reasonable ductility in single crystal forms. Though textured columnar grain structure has shown some ductility with 17% elongation [37], the polycrystalline forms in general have almost zero ductility [38]. The ductility of these alloys is influenced by various factors [39] :

- i) alloy compositions like Aluminium and boron levels.
- ii) alloy preparation and thermo mechanical treatment
- iii) trace impurities (such as oxygen and sulphur)
- iv) test environment
- v) grain size.

Figure 6 shows the variation of ductility with composition [10]. Considerable improvement can be seen with 0.02 wt% B though B in large quantities reduces the ductility and with 0.4 wt% B the second phase borides are seen and ductility falls below 10%. Variation of ductility with Al concentration in 0.05 wt% B doped alloy shows that ductility improves considerably in Ni-rich alloys. Al-rich alloys however remain brittle. Substitution addition like Pd are also seen to improve the ductility.

Though ductility of B-doped Ni_3Al shows an insensitivity to grain size at lower temperature, it fell appreciably with increasing grain size at higher temperatures. The one reason suggested for such behaviour is the formation of Ni-rich permeable oxide layer for coarser grains which changes to Al-rich impermeable layer for finer grain sizes. Various ways to improve

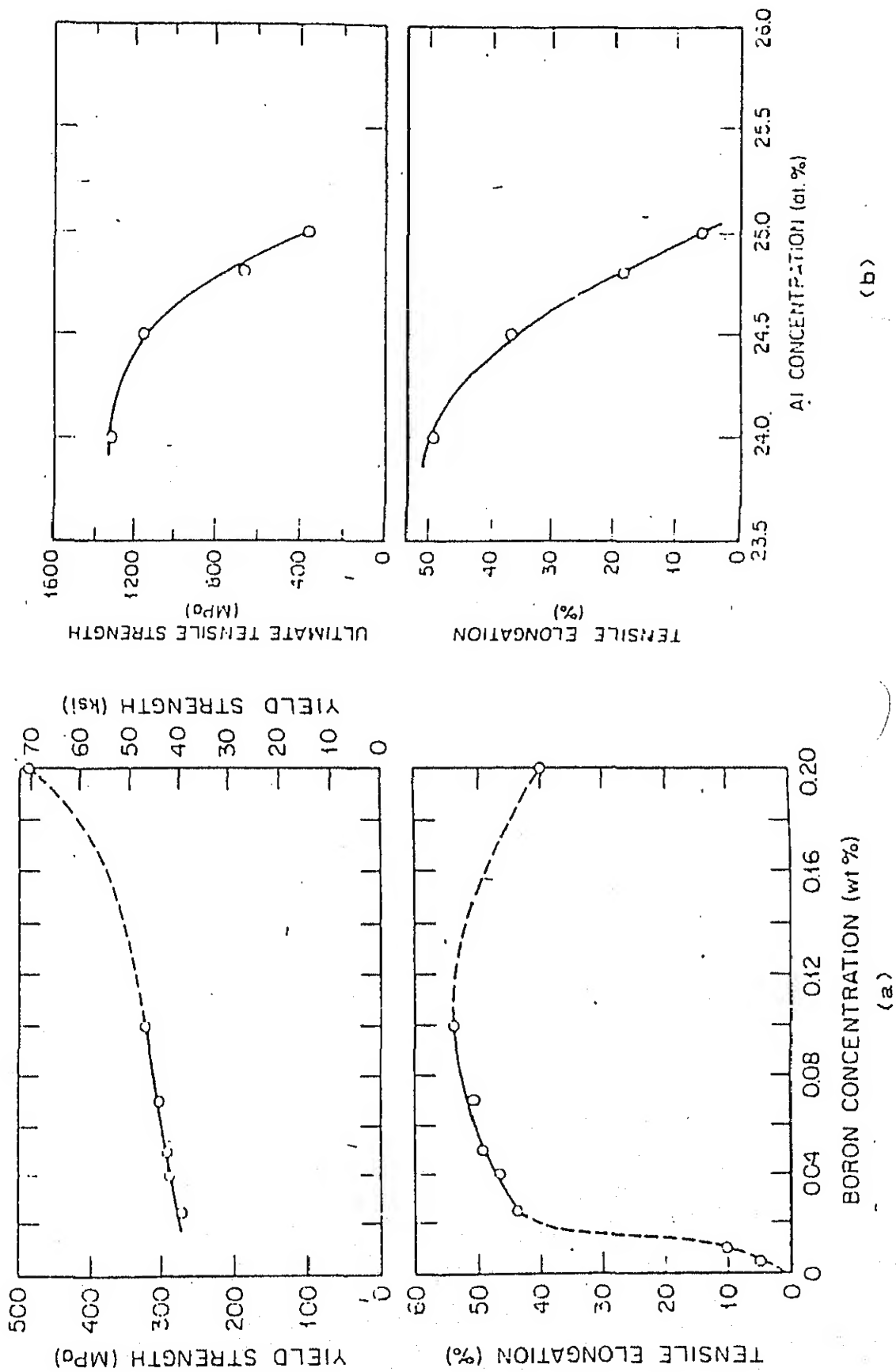


Fig.6 Plots of room temperature tensile properties as a function of (a) boron concentration in Ni-24Al (b) aluminum concentration in alloys doped with 0.05 wt% B.

ductility in B-doped Ni_3Al are available. Alloying with Cr [40] gives an oxide film shutting off path of gaseous oxygen from grain boundaries and base metal. Another way to change the oxidation resistance of material is to heat treat the material in such a way that composition of Ni-rich permeable oxide layer is affected [41].

Though ductility under standard constant strain rate test may be limited, the Ni_3Al alloys shows super plastic behavior [42]. The maximum elongation of 638% in Ni_3Al with 8 wt. % Cr was limited due to dynamic recrystallization.

2.5.3. Creep

One of the major barriers to the single phase Ni_3Al structures has been their low creep resistance contrary to the expectation of improved creep resistance due to ordered structure. Ni_3Al alloys shows lower resistance as compared to superalloys. The creep resistance can be increased with addition of solutes like Hf, Cr, Zr and Ta, obviously the coarser grain improving the resistance with other parameter being equal. Hf is particularly tried because it gives a simultaneous increase in the strength [43]. Study with various ternary additions in single crystal Ni_3Al [44] shows that Ni_3Al alloys may have creep resistance comparable with superalloy, although density advantage is lost.

2.6 Scope of Present Work

The review of literature shows that although thermo mechanical treatment of Ni_3Al is likely to improve its properties, this has not yet been tried. In this investigation, in order to investigate this aspect, rolling and recrystallization behaviour of Ni_3Al studied as a first stay.

CHAPTER 3

EXPERIMENTAL PROCEDURE

3.1 Alloy Preparation

3.1.1 Starting Materials

The starting materials for the alloys were nickel 99.99% purity, aluminium of 99.999% purity and crystalline boron chunks of 99% purity. The weight of component required for melting was taken directly from weight percent fraction without assuming preferential loss of any component.

3.1.2 Melting

The alloys were melted into buttons of about 20 grams weight in a non consumable tungsten electrode water cooled copper hearth arc melting furnace. Boron as a light element will float and can get lost during striking with arc. Further aluminium has a lower melting point than nickel and hence the stacking sequence of elements in the crucible was planned for boron, aluminium and on top, nickel. However with small button melts, the actual configuration was a large flat nickel piece in centre surrounded by other metallic pieces with boron at the bottom.

The furnace was evaluated and flushed with high purity argon before striking the arc. The alloy buttons were melted three times to ensure homogeneity. After each melting the button was turned over, the furnace evacuated and flushed with high purity argon. After melting, the buttons were weighed to obtain the weight loss.

3.1.3 Homogenization

The alloy buttons were vacuum sealed in fused silica tubes using a rotary pump to obtain a vacuum of the order of 10^{-8} torr. Based on the previous experience [45], a homogenization schedule of 1130°C for 5 days was followed. The homogenization was carried out in SiC vertical tubular furnace maintained within $\pm 2^{\circ}\text{C}$ using Indotherm proportional controllers. The ampoules were water quenched after homogenization.

3.1.4 Annealing

The beneficial effect of strengthening by boron can be seen if boron is allowed to segregate on grain boundaries. Slow cooling from higher temperature allows the boron to redistribute at grain boundaries [46]. A boron redistribution annealing was given to homogenized buttons in vacuum sealed ampoules as follows

1000°C for 1 hr $\xrightarrow[\text{In } 2.5 \text{ hr}]{\text{slow cool}}$ $500^{\circ}\text{C}/2 \text{ hr} \longrightarrow \text{Furnace Cool to Room Temp.}$

3.2 Recrystallization

3.2.1 Sample Preparation

2 mm thick slices were cut from the central portion of the button on a ISOMET low speed diamond saw. The slices were trimmed from all sides and polished to a rough finish. The rectangular slice thus obtained was viewed at low magnification to ensure that it is crack free to start with.

3.2.2 Rolling

Slices were rolled in a 2 high cold rolling mill. The roll gap was reduced slowly by about 400-500 μm in each pass.

Specimen was inspected for signs of cracks after each pass, till desired level of reduction in thickness could be obtained.

3.2.3 Recrystallization Annealing

The deformed slices were cut in three pieces, each piece was vacuum sealed in fused silica ampoules at vacuum $> 10^{-3}$ torr and were annealed at different temperatures in SiC tubular furnace. The temperature accuracy was $\pm 2^{\circ}\text{C}$. To study the time effect, cumulative time on a particular temperature, a particular piece has gone through was monitored by resealing the samples.

3.3 Optical Microscopy

After initial polishing on emery paper, samples were cold mounted and polished with 1μ alumina powder and etched. Etchant used was marble's Reagent consisting of 5g CuSO_4 , 20 ml HCl and 20 ml H_2O . Etching times of 25-30 second usually sufficed.

Quantification for the fraction recrystallized was carried out with the optical micrographs of recrystallized grains obtained. Volume fraction and area fraction were treated equal. Area fractions of the early stages of recrystallization were calculated by putting a transparent graph sheet with smallest square of 1 mm x 1 mm over the pictures. The points in 1 mm x 1 mm square which have recrystallized were counted over the whole picture areas. In later stages of recrystallization when large colonies of recrystallized grains were seen, the area fraction was calculated from the total areas of such colonies. The area viewed usually was $425\mu\text{m} \times 525\mu\text{m}$, though larger areas at a lower magnification were sometimes taken to avoid the discrepancy on

localized measurements.

3.4 Scanning Electron Microscopy

Scanning Electron Microscopy for the homogenized alloy was carried out on 25 kV JEOL Scanning Electron Microscope (SEM) attached with EDAX facilities. The samples prepared for optical microscopy were good and no additional preparations were made.

3.5 Differential Scanning Calorimetry

Differential Scanning Calorimetry (DSC) on the deformed samples were carried out on a computerised stanton Redcroft DSC 1500 system. Samples of 2.5 mm x 2.5 mm size were cut so that they could sit properly in alumina specimen crucibles. Undeformed specimen of the same size were used as a reference.

DSC cell was earlier calibrated both for heat flow rate and temperature using pure metals like indium and aluminium.

Isocronal annealing was carried out by heating in high purity argon atmosphere from 50°C to 1100°C at the desired heating rates. Isothermal studies were not carried out as sample temperature did not stabilise to a reasonable accuracy.

CHAPTER 4

EXPERIMENTAL RESULTS

4.1 Homogenized Alloy

Two alloys (designated as A and B in later parts), melted in two 20 gms buttons size did not show appreciable weight loss and the nominal compositions were accepted. A third alloy with lower weight loss was taken from a co-worker and is designated as 'C'. This alloy was also prepared in the same manner as 'A' and 'B'. The details about the compositions and weight losses on melting are given in Table 2.

Homogenized samples were annealed and examined in scanning electron microscope. The micro-structure showed homogenized structure and absence of 2nd phase particles. A typical micrograph is shown in Figure 7 for alloy 'C'. To ensure homogeneity, point analysis was carried out for different area using EDAX analysis. Ni-content did not vary from point to point. The large elongated grains in the homogenized structure were same as those commonly seen in the cast structure. A typical micrograph is shown in Figure 8.

4.2 Rolling Behaviour

Rolling behaviour of the alloys is summarised in Table 3.

Alloy A showed the rolling limit to be 12% when it is quenched in water after homogenization treatment. The rolling limit improves to about 15% when the annealing treatment described in section 3.1.4 is given after homogenization. Figure 9(a) shows the micrographs of alloy 'A' after rolling and annealing at 1000°C

Table 2
COMPOSITION AND WEIGHT LOSSES ON MELTING IN THE ALLOY BUTTONS
MELTED FOR PRESENT STUDY

Nomenclature	Composition atom %	wt %	Weight before melting	Weight after melting	weight-loss %
A	(Ni-24Al) _{99.9} B _{0.10}	Ni-12.6702Al- -0.0211B	20.4145 gms	20.3085 gms	0.519
B	(Ni-24Al) _{99.8} B _{0.20}	Ni-12.6675Al- -0.0424B	19.4984 gms	19.4059 gms	0.474
C*	(Ni-24Al) _{99.8} B _{0.20}	Ni-12.6675Al- -0.0424B	19.9129 gms	19.8971 gms	0.079

*Borrowed button segment.

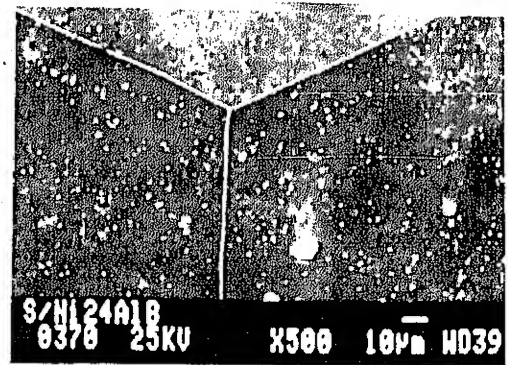


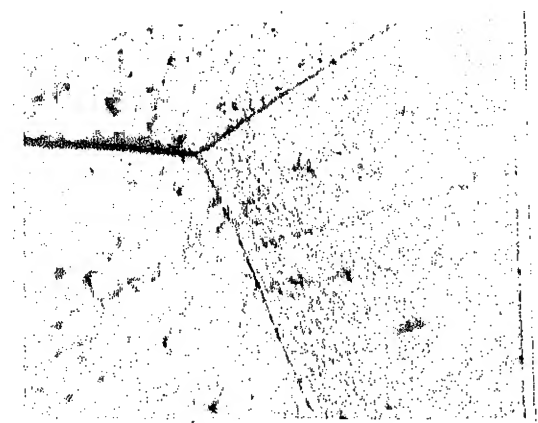
Fig.7 Scanning Electron Micrographs of structure of homogenized and annealed alloy 'C' at different magnification showing the single phase cast structure.



Fig.8 Micrograph showing structure of homogenized and annealed alloy 'C' showing the directionality of grains [x50]



(a)



(b)

Fig.9 Micrographs showing the structure of homogenised, annealed and 15% rolled alloy 'A' after a treatment at 1000°C for 1 hr (a) showing typical features of rolling (x70) (b) showing the deformation markings in the alloy [x350]

Table 3
ROLLING CHARACTERISTICS OF BORON DOPED Ni_3Al

Alloy Designation	Treatment	% reduction in thickness by rolling	Visual Examination
A	homogenized	~12%	Lot of Cracks both from inside as well as from the sides of the specimen.
	homogenized and annealed	~15%	Small number of cracks originating from the sides.
	homogenized, cold worked 15% rolled and annealed (at 1000°C 60°C followed by slow cooling	~8%	lot of cracks along the grain boundaries
B	homogenized and annealed	~20%	1 or 2 cracks in the middle of the specimen
C	homogenized and annealed	~30%	No cracks were seen on visual examination

for 1 hour. It shows the typical features of rolling. Figure 9(b) shows the deformation markings in the alloy rolled. Alloy 'A' rolled 15% and annealed could not take up further deformation exceeding 8% and heavily cracked. Figure 10 shows the grain boundary cracks in such alloys. It may be noted that all the cracks are inter granular in nature.

Alloy 'B' homogenized and annealed could be deformed to 20% reduction in thickness without major cracking. Alloy 'C' could be deformed to 30% reduction in thickness. Figure 11 shows the micrograph of the rolled structure. No visible cracks were there in the sample, but during later part of investigation, grain separation in one area was noted. Figure 12 shows the grain separation in alloy 'C' rolled by 30% and annealed at 850°C for 40 min.

4.3 Recrystallization

4.3.1 Alloy A - 15% deformation

Specimen of alloy A with 15% reduction was annealed for 1 hour at 1000°C and microstructure of the same is shown in Figure 9. It did not show any signs of recrystallization. Since higher deformations by rolling could not be given due to cracking, recrystallization work in this alloy could not be carried out.

4.3.2 Alloy B - 20% deformation

Figure 13(a) shows the microstructure of 1000°C for 15 minutes. It clearly shows the initial recrystallization. Recrystallization occurs primarily at grain boundaries and grain edges rather than grain centres. In 135 minutes at 1000°C , the specimen completely recrystallized (Figure 13(b)). Since this



Fig.10 Micrograph showing the structure of homogenised, annealed, 15% rolled and annealed alloy after 8% rolling showing intergranular crack [x 35].

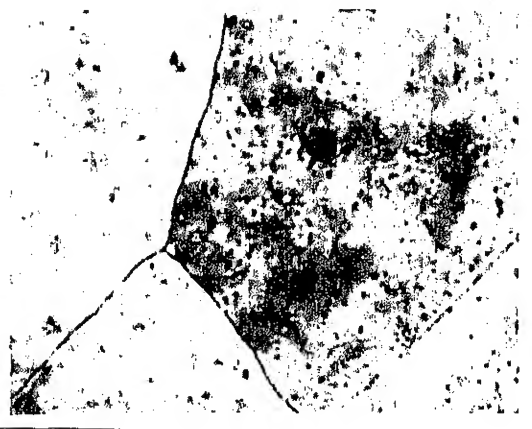


Fig.11 Micrograph showing the microstructure of homogenised and 30% rolled alloy 'C' showing the elongated grains [x 50].

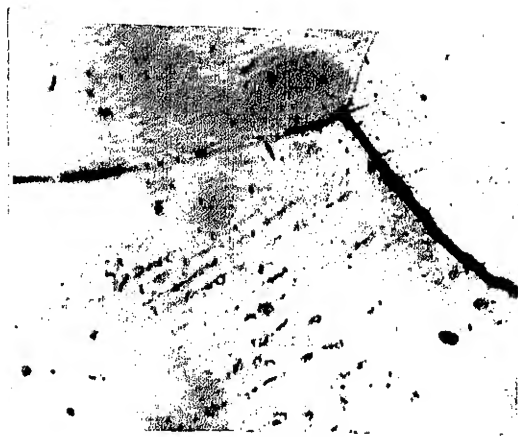


Fig.12 Micrograph showing the microstructure of 30% rolled and annealed ($850^{\circ}\text{C}/40\text{ min}$) alloy 'C' showing the grain separation. A few recrystallized grains are also seen [$\times 200$].



(a)



(b)

Fig.13 Micrographs showing the microstructure of 20% rolled alloy 'B' after a treatment at 1000°C for (a) 15 min. showing recrystallization at recrystallized grain boundary and grain edges (b) 135 min. showing almost complete recrystallization [$\times 70$]

CENTRAL LIBRARY
I.I.T. KANPUR

Acc. No. A.112807

material also showed visual cracks, the detailed recrystallization studies could not be carried out in this alloy.

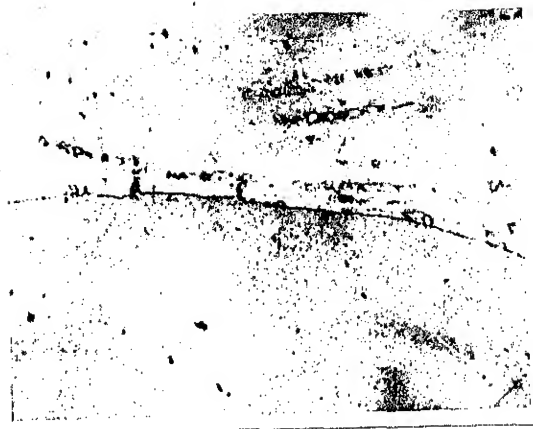
4.3.3 Alloy 'C' -30% deformation

Alloy 'C' did not show any visual cracks till 30% deformation and hence was used for detailed recrystallization studies.

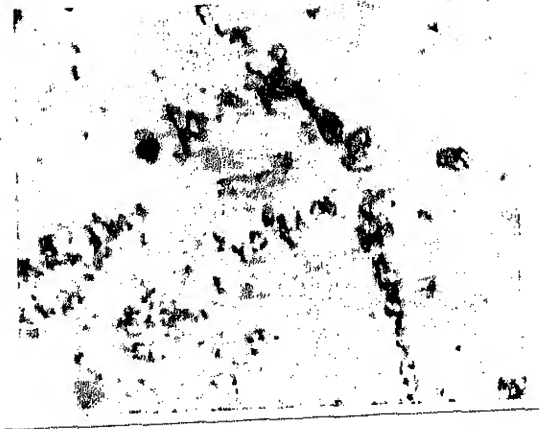
850°C : Figure 14 shows the progress of recrystallization at 850°C. 20 minutes of annealing at 850°C shows a very few nucleation of recrystallized grain mainly along the grain boundaries (Figure 14(a)). In 40 minutes, the tiny nuclei of recrystallized grains were clearly seen along the grain boundaries and on parallel lines within the grain (Figure 14 (b) and also Figure 12). Further increase in fraction recrystallized at 60, 80, 100 and 120 minutes was mainly limited to growth of the colonies at these sites (Figure 14 (c) to (f)). Note that Figure 14(d) shows different sizes of the recrystallized grains present in the same specimen. Figure 15 shows the micrograph at a lower magnification after 120 minutes and shows that though recrystallization has progressed considerably in many grains, it is absent in a few grains.

900°C : The progress of recrystallization at 900°C is shown in Figure 16. The recrystallization progresses from an average of 2.9% at 20 minutes to 47% at 60 minutes. In addition to the recrystallized grains at prior grain boundaries recrystallized grain colonies were seen in a few prior grains in parallel colonies within the grain (Figure 16(c)).

925°C : Progress of recrystallization was very fast. The specimens showed a considerable amount of recrystallization of



(a)



(b)



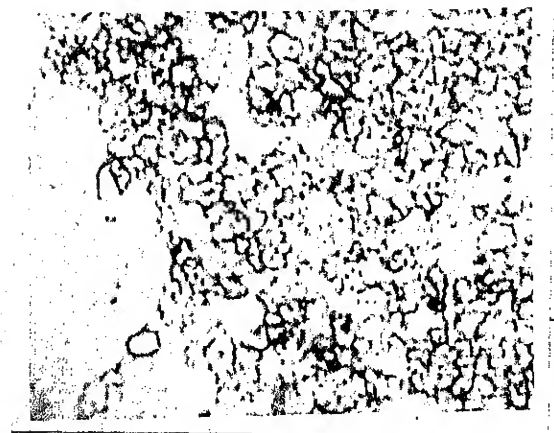
(c)



(d)



(e)

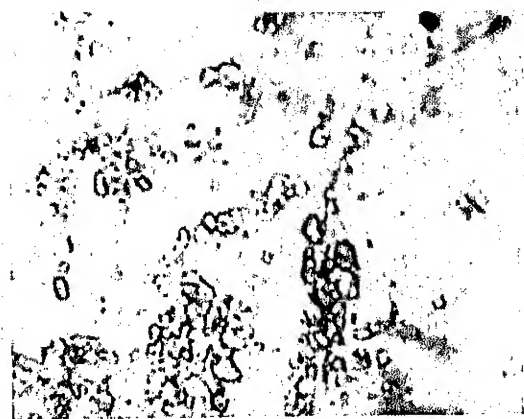


(f)

Fig.14 Micrographs showing the progress of recrystallization in 30% rolled alloy 'C' at 850°C (a) 20 min (b) 40 min (c) 60 min (d) 80 min. (e) 100 min (f) 120 min [x200]

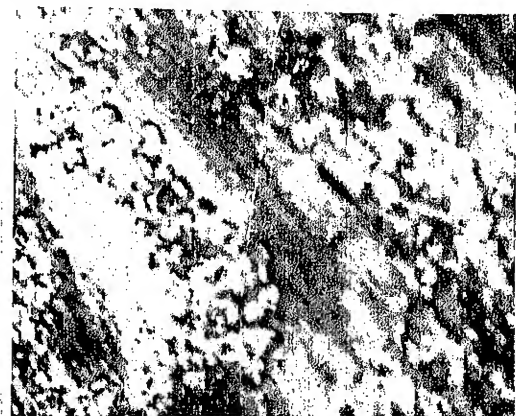


Fig.15 Micrograph of the structure of 30% rolled alloy 'C' after recrystallization at 850°C for 120 min. The recrystallization is absent in one grain [x 50]



(a)

(b)



(c)

Fig.16 Micrographs showing the progress of recrystallization in 30% rolled alloy 'C' 900°C for (a) 20 min (b) 40 min (c) 60 min [x200]

8.33% within 20 minutes (Figure 17(a)) and these specimens completely recrystallized within 1 hr (Figure 17(c)). The coarse sizes of 25 μm of recrystallized grains are seen here.

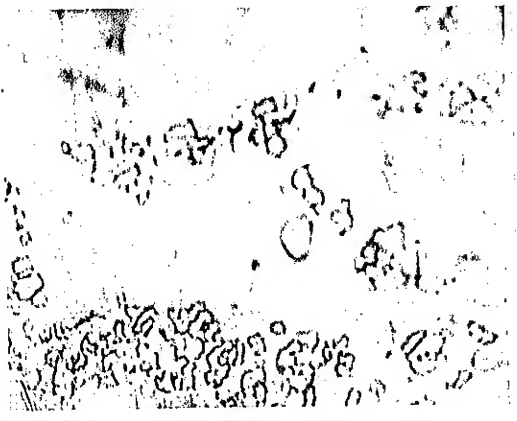
The fraction recrystallized at various temperature as a function of time is tabulated in Table 4. Fraction recrystallized as a function of time at various temperatures is also plotted in Figure 18.

4.4 DSC Measurements

Figure 19 shows the DSC plots obtained at 10, 15, 20 K/Min. constant heating rates for 20% rolled alloy 'B'. The onset of recovery is seen clearly by deviation from the base line.

The temperature range, over which recrystallization occurred, reduced with increasing heating rates. The 10K/Min. plot clearly that recrystallization progresses in different stages, though the stages are not separable at 20K/Min.

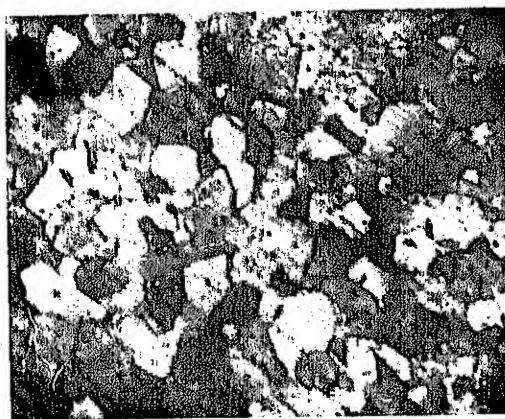
The heat released during the recrystallization was calculated to be about 3 cal/gm.



(a)



(b)



(c)

Fig.17 Micrograph showing the progress of recrystallization in 30% rolled alloy 'C' at 925°C for (a) 20 min (b) 40 min (c) 60 min [x200]

Table 4
 AREA FRACTION RECRYSTALLIZED AT VARIOUS RECRYSTALLIZATION
 TEMPERATURES WITH TIME

Alloy	Reduction in thickness (%)	Temperature (°C)	Time (min)	Area fraction recrystallized (in 425 x 525 μ m)		Average volume
				Area 1	Area 2	
A	15	1000	60	NIL	-	0.00
B	20	1000	15	0.20	-	0.20
		1000	135	1.00	-	1.00
C	30	925	20	0.085	0.081	0.083
			40	0.301	0.294	0.2976
			60	1.0	1.0	1.00
		900	20	0.030	0.028	0.029
			40	0.084	0.120	0.102
			60	0.461	0.479	0.470
		850	20	0.01	-	0.01
			40	0.042	0.067	0.05
			60	0.092	0.108	0.10
			80	0.192	0.209	0.20
			100	0.312	0.351	0.33
			120	0.615	0.586	0.60

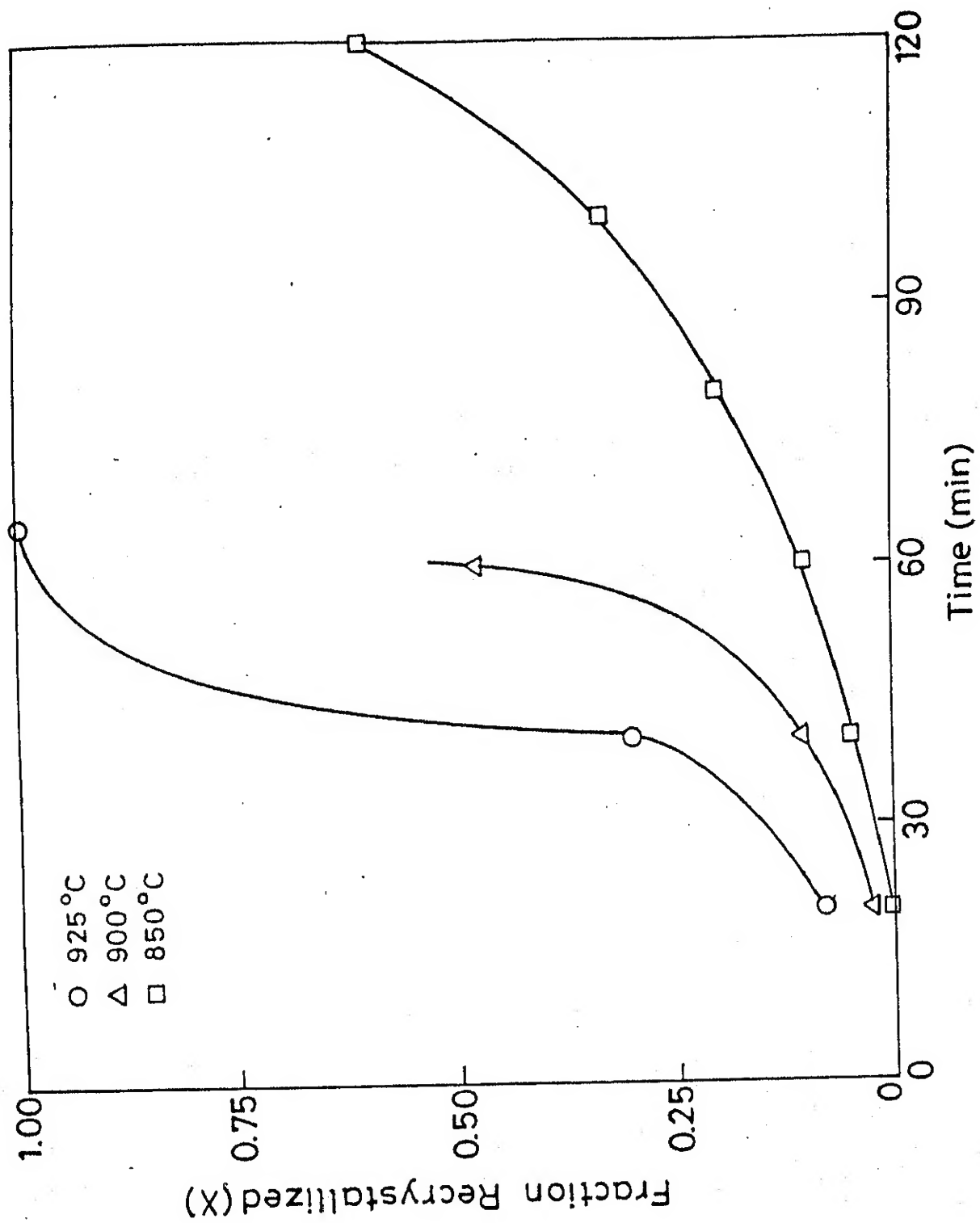
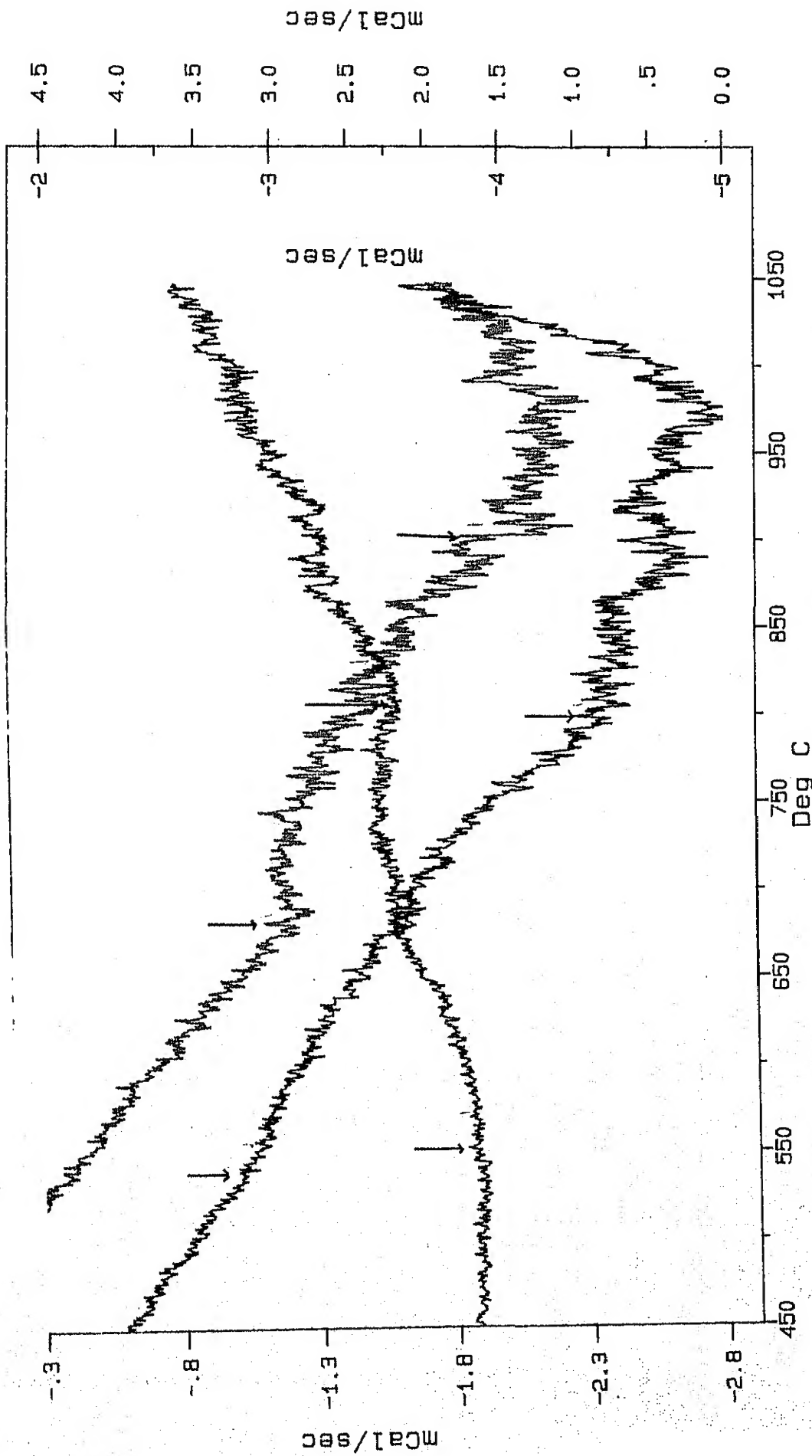


Fig.18 Plot showing the fraction recrystallized in 30% rolled alloy 'C' as function of time at various recrystallized temperatures.

COMMENT : R-26.6mg
 COMMENT : R-29.3 mg
 COMMENT : 23.9 mg

SMPL ID : R2 30%Rolled
 SMPL ID : R2-30
 SMPL ID : R2 30%Rolled

DSC 1500
 STANTON REDCROFT



Ramp 10 K/min. 15 K/min. 20 K/min. Onset of recrystallization
 Onset of recovery Fig 19 : DSC plots for 20Percent rolled alloy 'B' at different heating rates
 VERSION: C4.20.

CHAPTER 5

DISCUSSION

5.1 Rolling Deformation Behavior

Data listed in Table 3 show that homogenized alloy 'A' shows only 12% reduction in thickness. Annealing (see sec.3.1.4) does increase the percentage reduction in thickness. This is consistent with postulations [46] that slow cooling redistributes the boron to grain boundaries and thereby improves the ductility. Recrystallization treatment imparted to alloy 'A' with 15% reduction in thickness does not increase the percentage reduction. This is clearly due to the presence of cracks in the initial material.

Alloy 'B' contains 0.2 at% B compared with 0.1% in alloy 'A'. According to the reported variations of ductility with boron content (Figure 6), alloy 'B' should show higher ductility and indeed alloy 'B' could be deformed by 20% as compared to about 15% for alloy 'A'.

Alloy 'C' also contained 0.2 at% B in nominal compositions, but could be deformed by 30% reduction without visual signs of cracking. The relative response of these alloys to rolling is clearly due to the uncertain amount of boron which could be retained after melting. It is well known that during melting boron gets easily oxidized and evaporated. Therefore the amount of boron picked up remains uncertain. We had no means to determine the exact boron content of these alloys, however deformation behaviour suggests that in the alloy 'C', a larger amount of boron is retained, whereas in alloys A and B, boron loss is appreciable. The weight losses were also higher for alloys 'A'

and 'B' in the range of about 0.5% as compared to 0.08 % for alloy 'C'. It is observed in this investigation that cracks generally tend to initiate at the edges. When the specimen edges are ground, the crack propagation is quite suppressed. The failure was always due to intergranular cracks. Such grain boundary weakening has been observed in previous works also [10]. The presence of boron in 0.2 at % is reported to increase ductility to about 48% tensile elongation[10], whereas in best alloy 'C' deformation is estimated not to exceed 35% in view of the initiation of crack (Figure 12). This is probably due to the coarse grains of 300 μm present in the material in addition to the probability of lesser boron. Coarse grained material exposed to higher temperatures show a considerable loss of ductility due to oxygen pick up [47].

The recrystallization in various grains progresses at different rates as typically shown in Figure 15. One grain is completely free of recrystallization, whereas the others show appreciable amount of recrystallizations. This clearly suggests that all the grains are not deformed to the same extent. This has been observed in many systems [48, 49] including Ni_3Al [50]. The non-uniform deformations of grains can be explained due to the coarse grains having different orientation, thus the grains which are not suitably oriented, may not be deformed easily when the average deformation is 30%. As observed earlier that 15% deformation does not induce the recrystallization, it appears that recrystallization free grains in 30% deformed samples had a quite lower amount of deformation.

5.2 Recrystallization Behaviour

DSC curves (Figure 19) clearly show that in cold worked Ni_3Al , recovery occurs over a large temperature interval before initiation of recrystallization. The recovery processes are not thoroughly investigated. The recrystallization start at about 806°C at 10 k/min. constant heating rate. The metallographic studies show that around 850°C , the recrystallization rate is adequate for investigations by metallographic techniques and at temperatures about 925°C , is too high for accurate metallographic characterization.

Recrystallization is known to occur by nucleation and growth. In this investigation, primary nucleation sites have been grain boundaries, as shown in figures 14(b) and (d). Grain boundaries and grain corners have also been found to nucleate recrystallization (Figure 13(a)). This is expected as these are the high energy sites. Another important nucleation site observed is almost parallel rows of recrystallized grains into the prior grains (Figure 14(b) and Figure 12). This may be attributed to the defect produced within the grains by slip during deformation. Deformation bands were also the sites of nucleation as shown in Figure 16(c). Deformation bands are heavily deformed regions where the orientation differ appreciably from locations to locations within the grains. such regions are known to polygonise easily and elimination of two boundaries leads to the nucleation of strain free grains. This mechanism has been observed in a number of heavily deformed metals [51]. This observation confirms the earlier belief that some grains can get heavily deformed giving non uniform deformation of the material.

The mechanism of nucleation usually observed at low

deformations is due to strain induced migration of grain boundaries [51]. No evidence of this mechanism is however seen in our investigation.

Figure 17(c) shows the completely recrystallized microstructure. Here the average grain size is only about 25 μm as compared to the initial grain size of 300 μm in starting homogenized and annealed alloys. Thus recrystallization treatment can reduce the grain size considerably. It is known that finer grain sizes should improve the ductility [39]. The recrystallization should therefore be capable of giving better mechanical properties. Consequently thermomechanically treated Ni_3Al should produce better materials.

5.3 Kinetics of Recrystallization

Kinetics of recrystallization, being a nucleation and growth process is traditionally expressed by Jhonson-Mehl-Avrami equation [30]

$$X = 1 - \exp(-bt^n) \quad (1)$$

where X is the fraction recrystallized after time t, b is constant which depends upon both the nucleation and growth rates and n is Avrami exponent which depends upon the mechanism of recrystallization.

Eqn. 1 can be re written as

$$\ln[-\ln(1-X)] = \ln b + n \ln t \quad (2)$$

Eqn 2 shows that slopes of plots of $\ln[-\ln(1-X)]$ against $\ln t$ can be used to give the Avrami exponents. Data given in table 2 have been plotted as per eqn. 2 in Figure 20. At 850°C, all the points below 33% recrystallization fell on a straight line, as expected from the eqn. 2. At higher volume fractions,

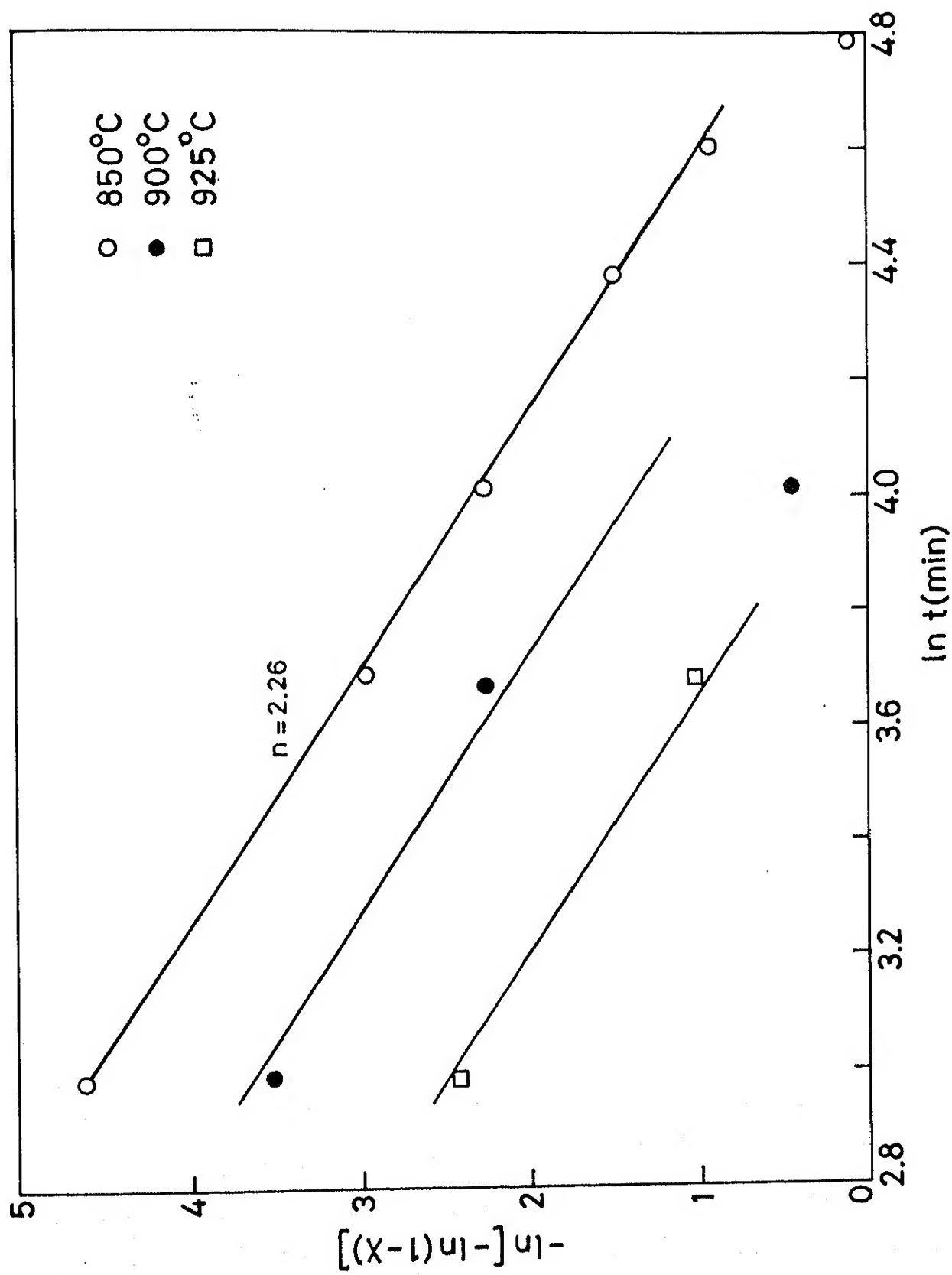


Fig.20 Plots of $-\ln[-\ln(1-X)]$ against $\ln t$ for calculation of Avrami exponent for recrystallization in 30% rolled alloy 'C' at different temperature.

the data deviated and could be approximated with another line with different slope. For the data points at 900°C and 925°C straight lines parallel to those obtained with data at 850°C have been drawn, due to lack of enough experimental data points at 900°C and 925°C . Avrami exponent for the lower fractions recrystallized was 2.26 and increased to about 3.5 for higher fractions. The value reported for 90% cold rolled B-doped Ni_3Al in earlier investigation [32] is 2.1 - 2.3. This is in excellent agreement with the value found in our investigation at lower volume fractions. The higher value of n at higher volume fractions is not reported in earlier study and might have been suppressed due to severe cold work.

During recrystallization, nucleation has been shown to occur at various high energy sites. The rate of nucleation is a function of free energy available for nucleation, however during recrystallization, recovery takes place simultaneously. The rate of nucleation must decrease rapidly at higher volume fractions recrystallized. Thus one may expect nucleation rate to be very high in the beginning, with a rapid fall with the progress of recrystallization. Consequently one may assume that most of the nuclei appear in the beginning and later contribution of the nucleation to the Avrami exponent should be negligible.

Linear growth is expected to occur during recrystallization. Linear growth rate is proportional to the free energy across the migrating transformation interface. As explained above, the recovery must decrease the growth rate with time. The contribution to the Avrami exponent from growth, therefore, must be less than 3 for 3-dimensional growth, but greater than 1.5 because growth is not parabolic initially. This

is consistent with the value of 2.26 observed in this investigation.

Nucleation in Ni_3Al occurs along grain boundaries and deformation bands with most of the nuclei appearing early in the transformation, while the progress of the recrystallization occurs by growth of available nuclei. The magnitude of the growth also seems to reduce with progress of recrystallization due to recovery.

Activation energy of the recrystallization can be calculated from the Arrhenius Relation.

$$t_x = t_0 \exp \left(\frac{Q_R}{RT} \right) \quad (3)$$

where t_x is the time to achieve volume fraction recrystallized x at temperature T . Plots of $\ln t_x$ against $1/T$ are used to calculate activation energy Q_R . Such plots for our investigation for various stages of recrystallization are shown in Figure 21. They yield activation energies of 1.23 - 1.52 eV, showing a slight increase with increasing recrystallization. The value compares well with value of 1.2 eV obtained earlier [32]. As compared to activation energy of diffusion of Ni in Ni_3Al i.e. 309 kJ/mol (3.2 eV), it is only 47% of activation energy of diffusion. Generally the activation energy for recrystallization is lower than that of diffusion. Defects produced during deformation tend to reduce the activation energy for diffusion. For example the presence of vacancies can reduce the activation energy of diffusion by as much as 50% [51]. The presence of dislocation etc. may therefore reduce the activation energy for recrystallization by providing an easier path for diffusion.

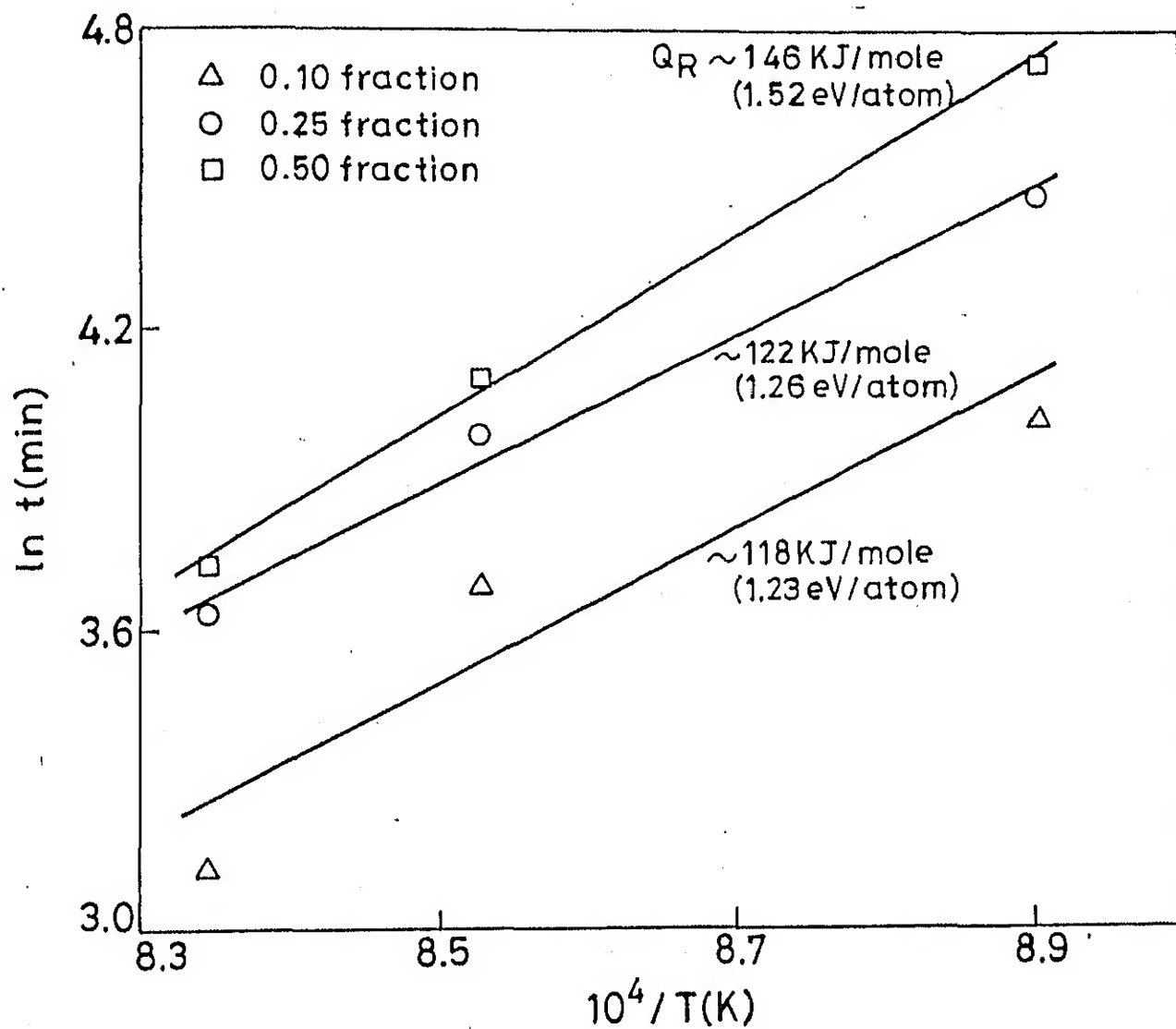


Fig.21 Plots of $\ln t_x$ against $1/T$ for various fractions recrystallized for recrystallization in 30% rolled alloy 'C'.

CHAPTER 6

SUMMERY AND CONCLUSIONS

1. Rolling behaviour of the homogenized alloys revealed that increase in boron content increases the ductility. The beneficial effect of boron is clearly shown if boron is redistributing to grain boundaries by slow cooling. Loss of boron during melting reduces the ductility, below the reported literature values.
2. Recrystallization occurs primarily at high energy sites like grain boundaries and deformation bands. The grain size refinements possible by recrystallization may be utilized to improve the mechanical properties via proper thermo mechanical treatments.
3. The kinetic of recrystallization can be described by Johnson-Mehl-Avrami equation. The possible explanation for the Avrami exponent obtained can be either the reduced nucleation, or reduced growth rates or both with the progress of transformation.
4. The activation energy for the recrystallization is about half the activation energy for diffusion of Ni in Ni_3Al . Though the process of recrystallization is quite complex for direct comparision of activations energies still the reduction can be explained by lesser resistance diffusion paths produced by deformation.

REFERENCES

1. M. Hansen and K. Anderko, "Constitution of Binary Alloys", 2nd edition, 1958, Mc Graw Hill, N.Y., p. 118.
2. P. Willemin, O. Dugue, M. Durrand, Charie and J.H. Davidson, Mat. Science & Tech. 2 (1986) 314.
3. S. Ochiai, Y. Oya and T. Suzuki, Acta Metallurgica 32 (1948) 289.
4. N.S. Stoloff, International Materials Review 34 (1989) 153.
5. D.M. Dimiduk, V.L. Weddington and H.A. Lipsitt, in "High Temperature Ordered Intermetallic Alloys II". Editor N.S. Stoloff, MRS Syp. Proc. 81 (1987) 221.
6. J.A. Horton, C.T. Liu and M.L. Santella, Met. Trans. 18A (1987) 1265.
7. P. Nash and D.R.F. West, Metal Science 15 (1981) 347.
8. T. Takasugi, O. Izumi and N. Masahashi, Acta Metallurgica 23 (1985) 1259.
9. L. Kaufman and H. Nesor, Canadian Metallurgical Quarterly 14 (1975) 221.
10. C.T. Liu, C.L. White and J.A. Horton, Acta Metallurgica 33 (1985) 213.
11. I. Baker, B. Huang and E.M. Schulson, Acta Metallurgica 36 (1988) 493.
12. S.C. Huang, A.I. Taub and K.M. Chang, Acta Metallurgica 32 (1984) 1703.
13. X.R. Qian and Y.T. Chen, Materials Letters 6 (1988) 157.
14. K. Aoki and O. Izumi, Physica Status Solidi 32a (1975) 657.
15. R.W. Guard and J.H. Westbrook, Trans. AIME 215 (1959) 871.
16. H.G. Hentzell, B. Andersson and S.E. Kalsson, Acta Metallurgica 31 (1983) 1131.
17. Y.G. Kim, Gi. W. Yoon and K.M. Chang, J. Mater Sc. Letters 4 (1985) 1407.
18. Y. Mishima, S. Ochiai and T. Suzuki, Acta Metallurgica 33 (1985) 1161.
19. J.A. Horton, C.C. Koch and C.T. Liu in "Proc. 41st Annual meeting : Electron Microscope Society of America" Editor G.W. Bailey, San Fransisco Press, (1983) 248.

20. R.W. Cahn, P.A. Siemers, J.E. Geiger and P. Bardhan, *Acta Metallurgica* 35 (1987) 2737.
21. L.Z. Zhuang, I. Majewski-Glabus, R. Vetter and J. Duszcyk, *Scripta Met. et Mater.* 24 (1990) 2083.
22. G.F. Hancock, *Physica Status Solidi* 7a(1971) 535.
23. M.B. Bronfin, G.S. Bulatov and I.V. Drugova, *Fizika Metall.* 40 (1975) 363.
24. K. Hoshino, S.J. Rothman and R.S. Averbach, *Acta Metallurgica* 36 (1988) 1271.
25. I. Baker, E.M. Schulson and J.R. Michel, *Phil Mag.* 57B (1988) 1815.
26. T.C. Chou and Y.T. Chou in "High Temperature Ordered Intermetallics Alloys" Editor CC Koch et al, MRS symp. Proc. 39 (1985) 461.
27. W.B. Hutchinson, F.M.C. Besag and C.R. Honess, *Acta Metallurgica* 21 (1973) 1685.
28. M. Gagne and E.M. Schulson, *Met. Trans.* 7A (1976) 1775.
29. I. Baker, D.V. Viens and E.M. Schulson, *J. Mater Sc.* 19 (1984) 1799.
30. J. Burke, "Kinetics of phase transformation in metals" Pergamon Press, Oxford, 1965.
31. G.R. Haff and EM Schulson, *Met. Tans* 13A (1982) 1563.
32. G.G. Gottstein, P. Nagpal and W. Kim, *Mater Sc. and Eng. A* 108 (1989) 165.
33. B.H. Kear and H.G.F. Wilsdorf, *Trans ASM* 59 (1966) 155.
34. E.M. Schulson, T.P. Weihs, D.V. Viens and I. Baker *Acta Metallurgica* 33 (1985) 1587.
35. R.D. Rawlings and A.E. Staton Bevan *J. Mater Sc.* 10 (1975) 505.
36. S.C. Huang, A.I. Taub and K.M. Chang, *J. Mater. Res.* 1 (1986) 60.
37. T. Hirano, *Acta Metallurgica* 38 (1990) 2667.
38. T. Ogawa, S. Hanada, T. Masumoto and O. Izumi *Met. Tans.* 16A (1985) 441.
39. M. Takeyama and C.T. Liu, *Acta Metallurgica* 36(1988) 1241.

40. C.T. Liu, in "MICON 86 : Optimisation of Processing, properties and service performance through microstructural control" ASTM STP 979 (1988) 22.
41. M. Takeyama and C.T. Liu, Scripta Met 23 (1989) 27.
42. A. Choudhury, A.K. Mukharjee and V.K. Sikka J. Mater. Sc. 25 (1990) 3142.
43. J.H. Schneibel, G.F. Peterson and C.T. Liu, J. Mater. Res. 1 (1986) 68.
44. D.M. Shah and D.N. Duhl in "High Temperature Ordered Intermetallic Alloys II" Ed. N.S. Stoloff, MRS Symp. Proc. 81 (1987) 411.
45. R.K. Ray, A.K. Jena and K.P. Gupta, "Thermodynamic Analysis and Structural Studies on the Stability of Intermetallics $L1_2$ and $B2$ such as Ni_3Al and $NiAl$: Report on DST Sponsored Project No. 11T-4(1)/86ET.
46. A. Choudhury, C.L. White and C.R. Brooks, MRS Proc. 122 (1988) 261.
47. M. Takeyama and C.T. Liu, Acta Metallurgica 37 (1989) 2681.
48. R.W.K. Honeycombe, "The Plastic Deformation of Metals" Edward Arnold, London, 1984.
49. W. Boas and M.E. Hargreaves, Proc. R. Soc. A 193 (1948) 89.
50. M.J. Mills, S.H. Goods, S.M. Foiles and J.R. Whetstone, Scripta Met. et. Mater. 25 (1991) 1283.
51. A.K. Jena and M.C. Chaturvedi, 'Phase Transformation' Prentice Hall, to be published

APPENDIX

ACTIVATION ENERGY

In order to test the internal consistency of the results, the activation energy has been calculated from the temperature dependence of the rate constant 'b' in Avrami equation (Equation 1).

The temperature dependence of the rate constant 'b' can be written as

$$b^{1/n} = \exp \left(- \frac{Q}{RT} \right) \quad (A1)$$

The equation 2 shows that value of b can be calculated from the plots of $\ln [-\ln(1-x)]$ against $\ln t$ when time t is extrapolated to zero.

The extrapolated values of $\ln b$ from Fig. 20 have been plotted in Fig. (A-1) against $1/T$. The slope $\frac{nQ}{R}$ of the plot gives $Q = 131$ KJ/mole which is quite consistent with activation energy calculated from Fig. 21.

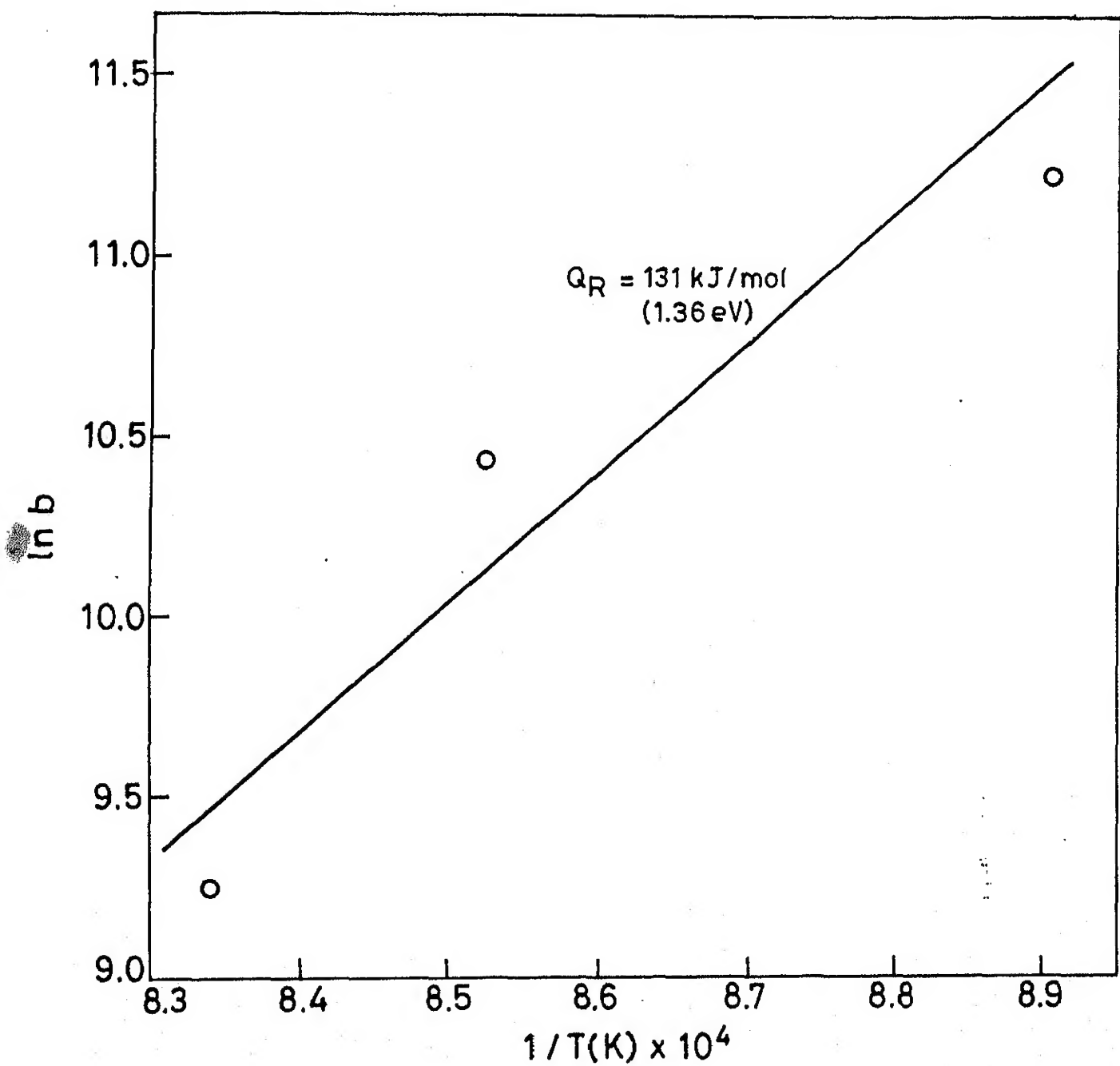


Fig. A1. Plot of $\ln b$ vs. $1/T$ for calculation of activation energy.

A 112807